PERMAFROST AND PERIGLACIAL PROCESSES
Permafrost and Periglac. Process. **27**: 324–338 (2016)
Published online 23 September 2016 in Wiley Online Library
(wileyonlinelibrary.com) DOI: 10.1002/ppp.1914

Remote Sensing of Landscape Change in Permafrost Regions

Mark Torre Jorgenson[1]* *and Guido Grosse*[2]

[1] Alaska Ecoscience, Fairbanks, AK, USA
[2] Alfred Wegener Institute Helmholtz Centre for Polar and Marine Research, Potsdam, Germany

ABSTRACT

Amplification of global warming in Arctic and boreal regions is causing significant changes to permafrost-affected landscapes. The nature and extent of the change is complicated by ecological responses that take place across strong gradients in environmental conditions and disturbance regimes. Emerging remote sensing techniques based on a growing array of satellite and airborne platforms that cover a wide range of spatial and temporal scales increasingly allow robust detection of changes in permafrost landscapes. In this review, we summarise recent developments (2010 – 15) in remote sensing applications to detect and monitor landscape changes involving surface temperatures, snow cover, topography, surface water, vegetation cover and structure, and disturbances from fire and human activities. We then focus on indicators of degrading permafrost, including thermokarst lakes and drained lake basins, thermokarst bogs and fens, thaw slumps and active-layer detachment slides, thermal erosion gullies, thermokarst pits and troughs, and coastal erosion and flooding. Our review highlights the expanding sensor capabilities, new image processing and multivariate analysis techniques, enhanced public access to data and increasingly long image archives that are facilitating novel insights into the multi-decadal dynamics of permafrost landscapes. Remote sensing methods that appear especially promising for change detection include: repeat light detection and ranging, interferometric synthetic aperture radar and airborne geophysics for detecting topographic and subsurface changes; temporally dense analyses at high spatial resolution; and multi-sensor data fusion. Remotely sensed data are also becoming used more frequently as driving parameters in permafrost model and mapping schemes. Copyright © 2016 John Wiley & Sons, Ltd.

KEY WORDS: remote sensing; landscape; change; permafrost; ecosystem; thermokarst

INTRODUCTION

Arctic amplification of global warming over the last few decades has led to significant changes in permafrost-affected landscapes (Serreze and Barry, 2011). Ecosystems in permafrost regions are diverse owing to strong gradients in environmental conditions and disturbance regimes, and they can be expected to show a broad range of responses to climate warming (Pearson *et al*., 2013; Jorgenson *et al*., 2015a). In Arctic and boreal biomes, changes to atmospheric, hydrologic, geomorphic, biotic and anthropogenic processes affect ecological patterns and processes and raise concern for ecosystem management and subsistence resources (Chapin *et al*., 2006). Permafrost fundamentally controls many ecological processes in northern landscapes because ground ice supports the surface and affects topography. The frozen ground also impedes soil drainage and subsurface water movement, leading to the prevalence of cold, wet soils with large organic carbon stores, and vegetation adapted to the extreme soil conditions (Grosse *et al*., 2011a; Schuur *et al*., 2015). Thus, permafrost is a critical component of the coupled atmosphere-ocean-land system that strongly affects the outcome of climate-induced changes.

The response of permafrost-affected landscapes to climate change since the 1970s is determined by the interaction of numerous factors. Increasing air temperatures have led to changing water balance and surface and subsurface hydrology (Walvoord *et al*., 2012). Permafrost degradation has increased (Grosse *et al*., 2011b), which radically reorganises hydrologic flow paths, soil processes, biogeochemical cycling and vegetation (Jorgenson *et al*., 2013). Compositional shifts or biomass changes in vegetation are occurring through altered nutrient availability and competitive interactions among plant species (Potter *et al*., 2013), snow cover change (Myers-Smith and Hik, 2013), herbivory (Joly *et al*., 2011) and thermokarst (Jorgenson, 2013).

* Correspondence to: M. T. Jorgenson, Alaska Ecoscience, Fairbanks, AK, USA. E-mail: ecoscience@alaska.net

Received 8 January 2016
Revised 21 April 2016
Accepted 28 June 2016

Increasing fire frequency and severity associated with climate warming may lead to a shift in forest and tundra composition and distribution (Barrett *et al*., 2011). Forest and shrub migration into new areas, altitudinal increases in treeline and shifts in dominance within plant communities have altered canopy dominance and understorey composition (Myers-Smith *et al*., 2011). Lake area has increased through shoreline erosion and decreased from drainage associated with permafrost degradation (Jones *et al*., 2011; Lantz and Turner, 2015), and evaporative loss and paludification (Roach *et al*., 2013). Sea ice retreat has led to increased storm surges, coastal erosion and salinisation (Lantuit *et al*., 2012a; Vermaire *et al*., 2013) and factored in broader ecological consequences (Post *et al*., 2013). Glacier melting has exposed new barren alpine areas subject to primary succession and permafrost formation, and affected the geomorphology of glacier-fed river systems (Moore *et al*., 2009). Increasing human populations and industrial activities in northern permafrost regions are fragmenting habitats (Kumpula *et al*., 2012; Raynolds *et al*., 2014). Collectively, these pulse (abrupt) and press (gradual) disturbances have produced a diverse mosaic of early to late-successional ecosystems (Chapin *et al*., 2006; Grosse *et al*., 2011a).

In this review, we summarise recent progress in the use of remote sensing to quantify how diverse environmental factors contribute to permafrost landscape change. We emphasise the extent and rates of landscape change, and the implications of these on permafrost stability, rather than focusing solely on remote sensing of permafrost, which has been the subject of recent reviews (Gogineni *et al*., 2014; Westermann *et al*., 2015a). We then consider specific permafrost degradation processes because of the fundamental importance of permafrost to northern ecosystems. Finally, we synthesise the rapidly expanding body of research to assess trends in landscape change, highlight sensors and methods that have facilitated progress, identify key challenges that remain and recommend approaches for improving remote sensing of permafrost dynamics. While hundreds of relevant studies have been published in recent years, we highlight only a fraction of them by focusing on those published during 2010–15.

LANDSCAPE CHANGES

Surface temperature is a critical factor affecting shrub and tree growth (Blok *et al*., 2011), vegetation structure and phenology (Xu *et al*., 2013), primary productivity and soil carbon balance (Schuur *et al*., 2015), glacier mass balance (Moore *et al*., 2009) and permafrost stability (Grosse *et al*., 2011b). Mean annual surface air temperatures from climate stations in the Arctic have increased by nearly 2 °C since 1900, with the majority of warming in autumn and winter (Serreze and Barry, 2011). The thermal bands from the Advanced Very High Resolution Radiometer (AVHRR) and Moderate Resolution Imaging Spectroradiometer (MODIS) with their sub-daily frequency have been widely used to map spatial and temporal variations of land surface temperatures (LSTs). Bhatt *et al*. (2013) used the AVHRR to reveal that trends in the summer warmth index (sum of degree months above freezing) from 1982 to 2011 varied by region, being positive around Alaska-Chukotka and negative over Eurasia and parts of northern Canada. Soliman *et al*. (2012) developed LSTs using Advanced Along-Track Scanning Radiometer (ENVISAT) and MODIS imagery to calculate weekly, monthly and annual LST means over the pan-Arctic region at various grid resolutions (1–25 km) for the past decade (2000–10). These satellite-derived LSTs are becoming increasingly important for assessing rates of ecological change (Bhatt *et al*., 2013) and providing input to permafrost models. Using MODIS LSTs, and other remote sensing and ground measurements, Langer *et al*. (2013) modelled surface heat transfer to estimate permafrost temperature and freeze-thaw dynamics in northern Siberia. Fusing data from MODIS LSTs, ERA-interim surface temperatures, MODIS Landcover and ERA snowfall data, Westermann *et al*. (2015b) modelled ground temperatures over a large Atlantic permafrost region at 1 km resolution using a simple semi-empirical equilibrium model.

Snow characteristics (timing, extent, thickness, water content) are critical for understanding permafrost thermal regimes because snow acts as a buffer between the atmosphere and ground in the winter, and interacts strongly with topography, hydrology and vegetation (Myers-Smith and Hik, 2013; Zeng and Jia, 2013). Remote sensing provides valuable tools for characterising snow on a wide range of scales. Global remote sensing data-sets of snow cover extent (SCE) and snow water equivalent (SWE) include optical MODIS products (250–1000 m resolution) and passive microwave radiometer products from the Scanning Multi-Channel Microwave Radiometer (55 × 41 km resolution), the Special Sensor Microwave/Imager (15 × 13 km) and the Advanced Microwave Scanning Radiometer (25 km resolution) (Hancock *et al*., 2013). The Cryoland Portal (<URL>http://www.cryoland.eu/) is a good example of how snow and ice products are readily accessible. Over northern permafrost regions, Muskett (2012) analysed 30 years of satellite microwave data to identify regional increases and decreases in SWE. Lindsay *et al*. (2015) studied the timing and duration of snow cover over Alaska, northwest Canada and the Russian Far East using MODIS, finding that snow cover duration ranged widely from 179 to 311 days/yr across these regions. Across the northern hemisphere, SCE has decreased by 7–11 per cent since the mid-1970s compared to the pre-1970s, with a significant decrease in spring (Brown and Robinson, 2011). Brown and Derksen (2013) found a 0.26×10^6 km^2/decade decrease in snow cover onset (October) for Eurasian SCE during 1982–2011. To target snow cover dynamics at higher spatial resolution, Macander *et al*. (2015) analysed 11 645 Landsat scenes from 1985 to 2011 to evaluate patterns of seasonal snow persistence in northwest Alaska. Snow cover has been recently mapped at very high resolution by Nolan *et al*. (2015) using aerial photographs and structure-from-motion

(SfM) technology. The emerging snow products are useful for analysing vegetation dynamics, and for modelling soil temperatures and permafrost distribution at regional and local scales. Assessing snow packs with remote sensing remains challenging, however, because of low spatio-temporal resolution and limited accuracy, especially for SWE, where sensor-specific results disagree.

Topography exerts an important control over hydrologic processes (Quinton *et al*., 2011) and in permafrost terrain is often related to ground-ice characteristics associated with periglacial microtopography (e.g. ice-wedge polygons) and thermokarst landforms (Jorgenson, 2013). Remote sensing of topography and surface deformation includes photogrammetric analyses of satellite or aerial stereo imagery, satellite or airborne interferometric synthetic aperture radar (InSAR), airborne light detection and ranging (LiDAR), SfM technology, as well as ground-based LiDAR and stereophotogrammetry. Hubbard *et al*. (2013) used airborne LiDAR, spectral metrics from WorldView-2 and geophysical data to characterise microtopography associated with ice-wedge polygons, active-layer thickness and underlying permafrost near Barrow, Alaska. Paine *et al*. (2013) used green-wavelength airborne LiDAR to map lowland topography, including the bathymetry of shallow thermokarst lakes and streams in northern Alaska. Jones *et al*. (2013a) used repeat LiDAR (2006, 2010) to detect significant subsidence (>0.55 m) over 0.3 per cent of a 100 km^2 coastal strip in northern Alaska related to shoreline erosion, ice-wedge degradation and thermal erosion gullies. Repeat LiDAR also was used by Jones *et al*. (2015) at the site of the Anaktuvuk River tundra fire to map thermokarst subsidence in 34 per cent of the burned area versus 1 per cent of unburned areas within 7 years. Subsidence of > 1 m was detected over ice wedges. Kizyakov *et al*. (2015) derived digital elevation models (DEMs) through stereo-photogrammetric analyses of WorldView-1 images to quantify changes in a pingo-like mound and subsequent formation of a large crater on the Yamal Peninsula. Multi-temporal elevation models based on stereo-photogrammetric analyses of high-resolution aerial and satellite imagery allowed Günther *et al*. (2015) to

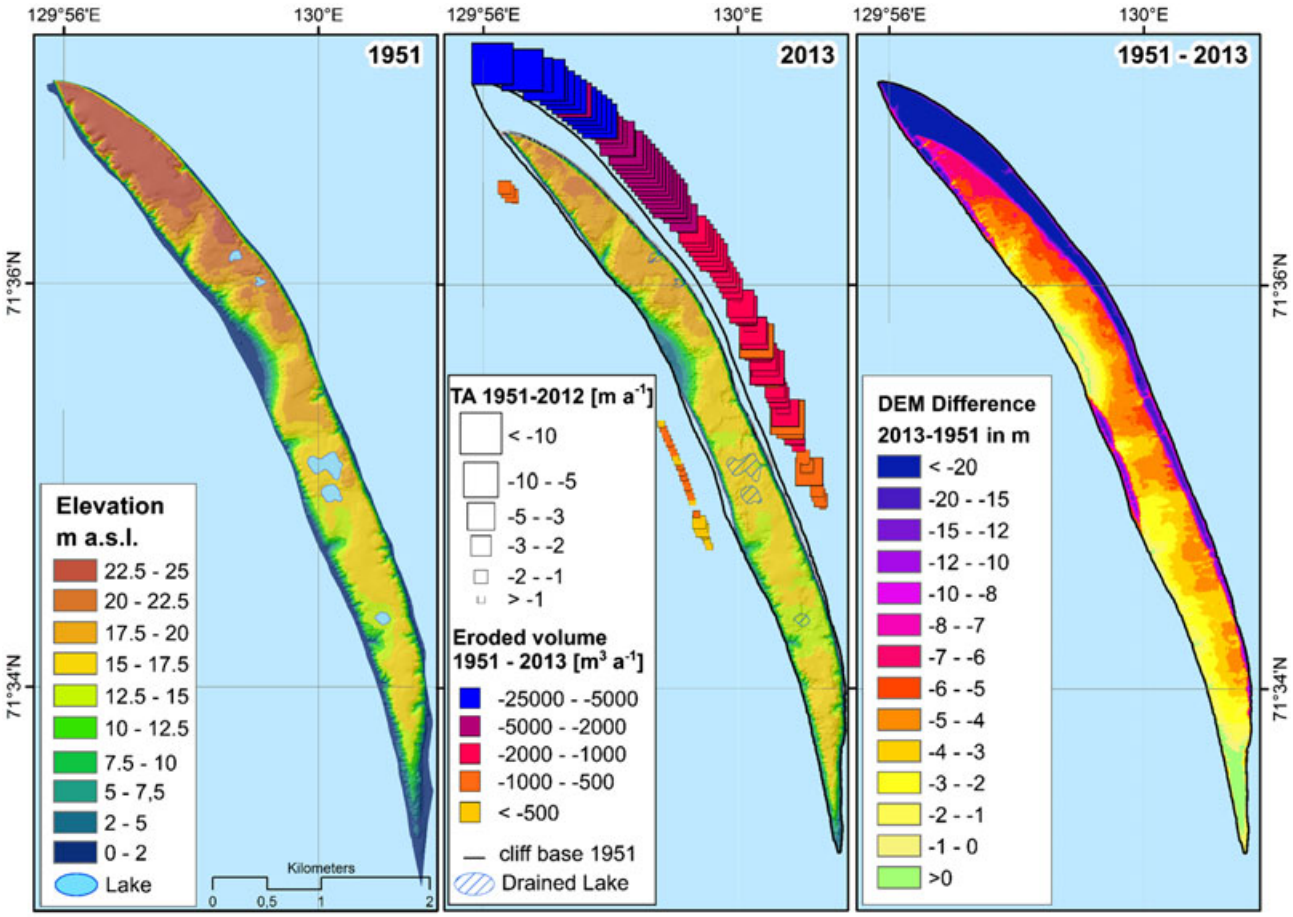

Figure 1 Coastal erosion and surface subsidence on Muostakh Island in the southern central Laptev Sea determined through stereo-photogrammetric generation of digital elevation models (DEMs) using: (left) 1951 aerial photography; and (middle) 2013 GeoEye stereo pair (from Günther *et al*., 2015). Symbol size represents the planimetric coastal erosion rate, while colour represents volumetric erosion rates.

detect surface subsidence averaging 5.8 cm/yr over 62 years on the ice-rich Muostakh Island in the Russian Arctic (Figure 1). Kääb *et al*. (2014) applied photogrammetric SfM technology to monitor periglacial microrelief and sediment movement in sorted circles due to freeze-thaw processes at millimetre resolution on Svalbard. The use of drones for creating digital surface models and monitoring vegetation shows high potential for assessing impacts from permafrost degradation (Fraser *et al*., 2015). Other studies have advanced InSAR methods for permafrost terrain by quantifying seasonal surface elevation changes at centimetre resolution associated with freeze-thaw dynamics of the active layer (Liu *et al*., 2012; Li *et al*., 2015), or long-term subsidence associated with permafrost thaw (Chen *et al*., 2013; Liu *et al*., 2014). The rapid advance in high-resolution techniques for quantifying surface deformation during the last 5 years is extraordinary.

Surface water provides fish and waterbird habitats, serves as a water source for humans and strongly influences permafrost stability, as well as energy and trace gas fluxes between the land and atmosphere with potential feedbacks to landscapes and climate change (Roach *et al*., 2013; Walter-Anthony *et al*., 2014). Analysing changes in surface water, however, is complicated by the size of waterbodies in relation to image resolution, seasonal variations in depth and ice cover, and regional differences in factors driving change. Carroll *et al*. (2011), using 250 m MODIS from 2000 to 2009 to map water bodies across Canada, showed an overall areal reduction of 6700 km^2, with modest gains in boreal regions being offset by large losses in the Arctic. In contrast, Lu and Zhuang (2011) used multivariate methods on a Landsat time series to determine that water surface area decreased by 12.6 per cent from 1984 to 2003 in the boreal-dominated Yukon River watershed. Using a Landsat time series, Roach *et al*. (2013) found landscapes in boreal Alaska with both increasing and decreasing surface water extent, with declining areas more associated with fires (presumably affecting permafrost), coarser soils and farther from rivers. Lantz and Turner (2015), using airphotos and satellite imagery from 1951 to 2007, found a ~ 6000 ha decline in total lake area in the Old Crow Flats, driven mostly by the drainage of large lakes. Measurement of water extent, however, is affected by image resolution and small water bodies are particularly important in permafrost landscapes (Muster *et al*., 2013). In an Arctic landscape in northwest Alaska, Jones *et al*. (2011) found that the number of large lakes (>40 ha) decreased by 26 per cent from ~ 1950 to ~ 2006, while total water area (including small water bodies) decreased by only 15 per cent, with the number of small water bodies increasing by 11 per cent. Analysis of surface water at high latitudes based on AVHRR imagery from 2003 to 2011 showed water extent to be seasonally variable, with maximum summer coverage varying as much as 7 per cent from long-term means across regions (Watts *et al*., 2012). Similarly, Tarasenko (2013) used 2000–09 Landsat imagery to show that water extent in thermokarst lakes varied as much as 33 per cent from June to August and found large differences among years. Use of moderate-resolution synthetic aperture radar (SAR) imagery for monitoring wetlands also shows good potential (Reschke *et al*., 2012; Trofaier *et al*., 2013). Finally, good progress has been made in using Landsat and MODIS imagery for monitoring seasonality of Arctic lake ice (Hinkel *et al*., 2012; Arp *et al*., 2013), and for using lake ice patterns to map shallow lake bathymetry (Grunblatt and Atwood, 2014). Given the large seasonal and spatial variation in water characteristics, a huge challenge remains in assessing long-term trends and causative factors.

Vegetation biomass and structure are fundamental components of northern ecosystems and habitat use (Joly *et al*., 2011), and influence permafrost stability by affecting the radiation budget (Chapin *et al*., 2006), snow distribution and soil temperatures (Myers-Smith and Hik, 2013). Using the normalised difference vegetation index (NDVI), which is strongly correlated to above-ground vegetation biomass, Epstein *et al*. (2013) found that Arctic tundra biomass increased 20 per cent over a 29 year period (1982–2010) based on AVHRR data. Bhatt *et al*. (2013), using 8 km resolution NASA Global Inventory Modeling and Mapping Studies (GIMMS) data, found steady increases in the maximum NDVI across Eurasia, western North America and eastern North America over the 1982–2011 period, even though trends in the summer warmth index among regions were inconsistent. Beck and Goetz (2011) compared NDVI data from GIMMS and MODIS and found that the trends of increasing tundra and decreasing boreal forest productivity have amplified in recent years, particularly in North America, with decreases in boreal forest productivity most prominent in evergreen forests. Zeng and Jia (2013), using MODIS (2000–10) for the Yamal Peninsula, Russia, found that the start of the growing season became later over the course of the decade. Blok *et al*. (2011) found that the NDVI increased, and albedo decreased with increasing deciduous shrub cover. When using high-resolution Landsat data (1985–2007) for detecting NDVI trends for the foothills of northern Alaska, Raynolds *et al*. (2013) found that 5 per cent of the area had a significant increase and 0.4 per cent had significant decreases, with the heterogeneous patterns related to terrain conditions. Using Landsat (1986–2009) for interior Alaska trends, Baird *et al*. (2012) found declining NDVI trends across floodplain, lowland and upland landscapes. LiDAR has been increasingly used to quantify vegetation structure, for example, Selkowitz *et al*. (2012) combined ICESat Geosciences Laser Altimeter System LiDAR, Multi-Angle Imaging Spectroradiometer and MODIS imagery to map canopy heights in boreal forests over interior Alaska.

Land cover classification and mapping is important for quantifying vegetation and soil characteristics, partitioning the geographic variability of environmental properties and providing baseline data for assessing climate and permafrost interactions. To map Arctic vegetation, Walker *et al*. (2002) incorporated vegetation structure and composition to differentiate15 classes at a small scale, based on photo-interpretation of AVHRR satellite images. For the circumboreal region, an international effort is underway to

classify and map boreal vegetation through manual delineation of MODIS imagery (Saucier *et al*., 2015). MODIS imagery was used to develop land cover maps of Canada with 39 classes (Latifovic *et al*., 2014) and Russia with 72 classes and additional database-linked subdivisions (Schepaschenko *et al*., 2011). Higher-resolution mapping with Landsat imagery has been done for northern Alaska with 24 classes (Ducks Unlimited, 2013), northwest Alaska with 44 ecotypes (Jorgenson *et al*., 2015a) and Arctic Canada with 15 classes (Olthof *et al*., 2009). Given the strong relationships among vegetation-soil-permafrost properties, analysis of landscape trends needs to make better use of land cover maps.

Land cover change affects the surface energy budget with implications for feedbacks to the global climate system (Loranty and Goetz, 2012), primary productivity and soil carbon balance (Schuur *et al*., 2015), and wildlife use (Jorgenson *et al*., 2015a). Potapov *et al*. (2011) used Landsat to show that forest cover was reduced by 1.5 per cent within European Russia from 2000 to 2005. Fraser *et al*. (2014) used a Landsat time series covering the Mackenzie Delta region to create temporal profiles of tasselled cap brightness, greenness and wetness indices to differentiate disturbance-related trends in post-fire succession, drained lake succession and shoreline erosion. By photo-interpreting vegetation and landforms on high-resolution aerial photographs (~1980, ~ 2009) in northwestern Alaska, Swanson (2013) found that 24 per cent of 206 sites showed changes in vegetation structure, primarily due to shrub expansion (7%), floodplain succession (2%), tree increase due to post-fire succession (5%) and thermokarst lake increases (3%). Jorgenson *et al*. (2015) used a Landsat-derived map of 43 ecotypes in northwest Alaska, developed from field landform-vegetation-soil relationships and historical trends determined from photo-interpretation of ~ 11 000 point locations, to project modest net changes ($6-17\%$) in ecotypes by 2100 (mostly from shrub and tree expansion, fire, succession and thermokarst) based on transition probabilities related to time and temperature. In contrast, Pearson *et al*. (2013) used a climate envelope-type model using the CAVM map to project that vegetation in $48-69$ per cent of the Arctic will shift to a different class by the 2050s under various climate change scenarios. Lin *et al*. (2012) classified seven land cover types on a time series of historical aerial photographs (1948, ~ 1980) and Quickbird images (2002–08) and found that Alaska sites became drier and shrubbier, while Chukotka sites became wetter, and shrub tundra expanded wherever present. These data provide a wide range of estimates in historical and projected changes, revealing challenges in comparing data analysed using differing imagery, scales, classification systems and regions.

Shrub and forest expansion into tundra regions, a specific type of land cover change, is receiving increased attention because it is perceived as an early indicator of ongoing ecosystem shifts in a warming Arctic (Myers-Smith *et al*., 2011). Urban *et al*. (2014) used Landsat MSS data from 1973 and RapidEye images from 2012 to map small northward expansion of woody vegetation on the Taymyr Peninsula, Russia. Frost and Epstein (2014), using point sampling and photo-interpretation of old satellite photography (Gambit and Corona, 1965–69) and recent very high-resolution imagery (GeoEye, WorldView), found that alder shrub cover increased 1.3–6.0 per cent per decade across five sites in northern Siberia. Lantz *et al*. (2013) mapped tall shrubs in the uplands of the Mackenzie Delta region using 1972 and 2004 aerial photographs and found that shrub cover increased by 15 per cent. Beck *et al*. (2015) analysed a Landsat time series (1986–2008), Quickbird (2004) and GeoEye (2009) images for subarctic Québec and detected a 21 per cent increase in spruce forests and tall shrubs at the expense of low vegetation. An increase from 34 to 44 per cent in the extent of dense shrubs and forest in Québec also was found by Tremblay *et al*. (2012), based on the interpretation of 1964 and 2003 aerial photographs for a small area. Naito and Cairns (2015) used semi-automated image classification of historical aerial photographs (1950s, 1980s) and high-resolution satellite imagery (QuickBird, WorldView, GeoEye, Ikonos) to map shrub patches in nine study areas in northern Alaska and found that mean shrub cover across all sites increased from 28 per cent in ~ 1977 to 37 per cent in ~ 2009. Shrub growth has been shown to be highly correlated with remotely sensed NDVI, but growth varied across landscapes in Québec (Ropars *et al*., 2015). Blok *et al*. (2011) showed that shrub canopies reduce ground heat flux and active-layer depths, while Lawrence and Swenson (2011) found that increased shrubs can increase snow depths, and thus reduce albedo and increase soil temperatures. The interacting effects lead to substantial uncertainty as to how shrub and forest expansion will affect surface energy fluxes and permafrost stability (Loranty and Goetz, 2012).

Fire is an important disturbance process in boreal (Kasischke *et al*., 2010) and Arctic regions (Rocha *et al*., 2012) that initiates secondary succession, reduces surface organic layer thickness and carbon storage, and affects energy exchange, soil temperatures and permafrost stability (Jafarov *et al*., 2013; Jones *et al*., 2015). Severe fire seasons in Alaska in 2004 (2.7 M ha burn area) and 2015 (2.1 M ha), in Canada in 2015 (4.0 M ha), and in 2012 in Russia (30 M ha) have led to concern of increased fire frequency in response to climate warming (Kasischke *et al*., 2010). Loranty *et al*. (2014) found that while some of the best-documented tundra fires are located in Alaska, a large proportion of global tundra fires actually happen in Russia, with an average annual area burned of 331 200 ha/yr in Russia versus 21 400 ha/yr in Alaska for 1950–2011. Beck *et al*. (2011) used MODIS imagery to calculate the deciduous fraction of burn scars and normalised burn ratio, along with maps of burned areas, albedo and forest biomass, to conclude that more severely burned areas in interior Alaska since the 1950s have shifted toward greater deciduous biomass. An assessment of vegetation succession along the century-scale chronosequence of tundra fire disturbances from 1880 to 2007 manually interpreted using satellite imagery from arctic Alaska found that tundra fires facilitated shrub expansion (Jones *et al*., 2013b). An unusually large

tundra fire in northern Alaska has led to substantial organic matter loss and widespread thermokarst (Liu *et al*., 2014; Jones *et al*., 2015). Lantz *et al*. (2013) found that areas on 2004 aerial photographs that were burned between 1960 and 1968 had much higher shrub cover (92–98%) compared to unburned areas. In addition, their field measurements showed that alder-dominated sites had decreased albedo and snow pack and increased net solar radiation and ground temperatures, indicating that increasing shrub cover can affect regional climate and permafrost stability. Lu and Zhuang (2011) found little overall change in forest or shrub cover over a nearly three decade period in the Yukon River basin based on analysis of Landsat imagery. The steady land cover composition over time was attributed to post-fire succession across disturbance patches of varying age, despite high fire frequency.

Human activity associated with oil and gas development, mining, hydroelectric dams, forestry, agriculture, human settlements, and subsistence hunting and fishing are having increasing impacts on northern ecosystems (Chapin *et al*., 2006). Raynolds *et al*. (2014) used a time series of infrastructure mapping and aerial photograph analysis (1949–2011) to determine that direct and indirect oilfield impacts had affected 34 per cent of the mapping area. Walker *et al*. (2009), using the AVHHR-derived NDVI for the Yamal Peninsula, concluded that gas field infrastructure was not extensive enough to affect regional NDVI patterns, and that the impacts of massive reindeer herding were difficult to assess due to a lack of unaffected control areas. Kumpula *et al*. (2012) manually interpreted and digitised anthropogenic impacts on the Yamal Peninsula using Landsat, SPOT, Advanced Spaceborne Thermal Emission and Reflection Radiometer, Quickbird and GeoEye imagery from 1984 to 2011 to show that visibly affected areas increased from 70 to 836 km^2, with a sharp increase after 2004, associated with a wide range of oil development activities. In assessing the overall extent of human development in Alaska, Selkowitz and Stehman (2011) processed Landsat imagery to determine that urban development and agriculture affected only 0.1 per

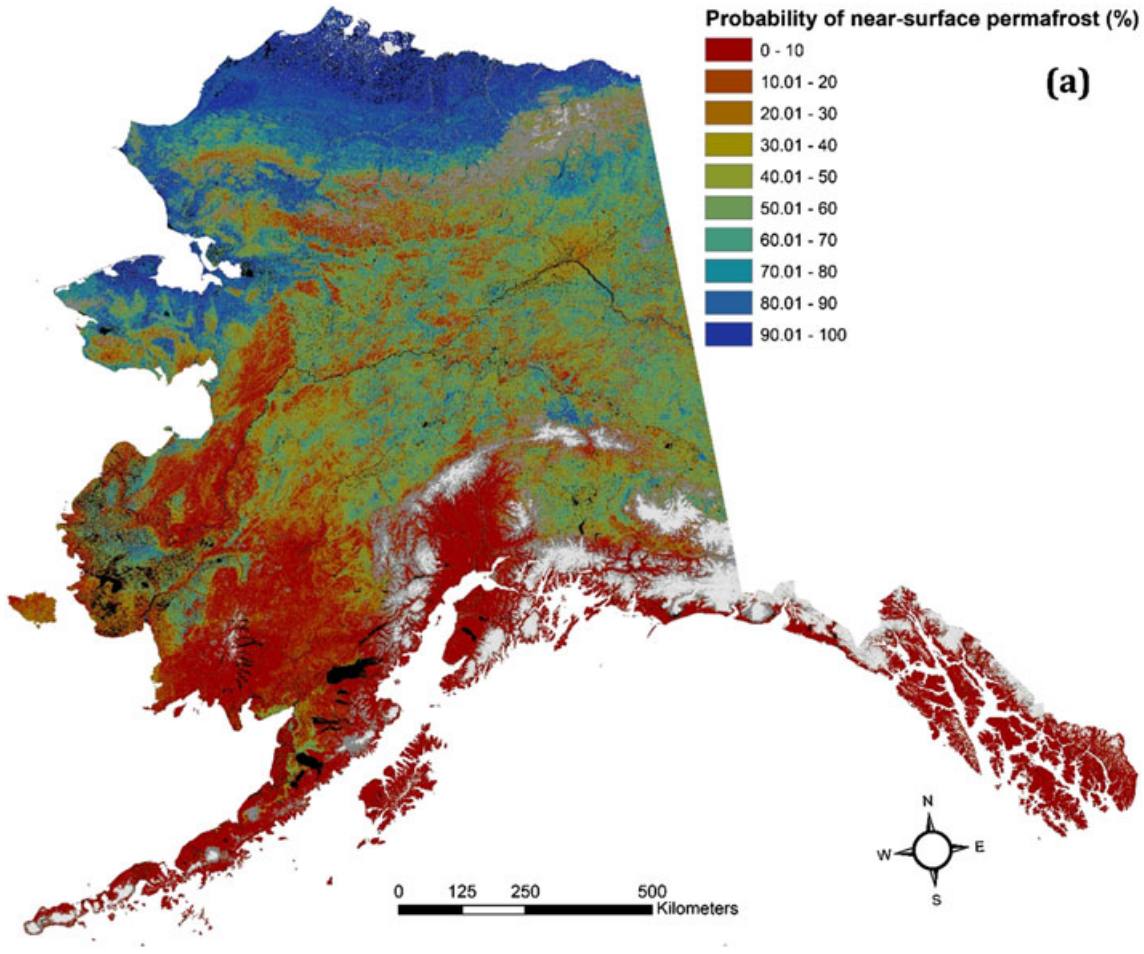

Figure 2 Landsat-derived map of probability of near-surface (within 1 m) permafrost in Alaska based on multivariate modelling involving spectral indices, terrain components and a large ground data-set (from Pastick *et al*., 2015).

cent of the region. While the overall extent of human activity is relatively small, the impacts can cause substantial disturbances of local permafrost (Raynolds *et al*., 2014).

PERMAFROST DEGRADATION

Permafrost mapping allows insights into current ecosystem dynamics and feedbacks and provides a baseline for assessing future landscape change and permafrost degradation. Permafrost distribution has been mapped using thermal modelling (Jafarov *et al*., 2012; Slater and Lawrence, 2013), LSTs from MODIS imagery (Westermann *et al*., 2015b), empirical statistical modelling using Landsat and SPOT spectral indices and terrain characteristics (Panda *et al*., 2012; Pastick *et al*., 2015) (Figure 2), snow basal temperatures in conjunction with land cover maps (Bonnaventure *et al*., 2012), manual interpretation of Landsat imagery based on permafrost-landform relationships (Jorgenson *et al*., 2015) and airborne electromagnetic resistivity (Minsley *et al*., 2012; Pastick *et al*., 2013). In a notable data fusion approach, Zhang *et al*. (2014) integrated a high-resolution land cover map derived from SPOT imagery, field measurements and a process-based model to map permafrost and project future distribution in response to climate warming. Some of the mapping approaches have been used to simulate permafrost distribution over the 21st century and all agree that large decreases in permafrost extent can be expected in response to projected climate warming (Jafarov *et al*., 2012; Slater and Lawrence, 2013; Panda *et al*., 2014; Pastick *et al*., 2015). However, due to differences in methods and how the models parameterise landscape characteristics, there is substantial variability within and among these spatial models.

Permafrost degradation directly affects surface topography through thaw settlement and hydrologic redistribution by altering surface flow, soil infiltration and subsurface pathways. These changes then have large consequences on energy balance and soil temperatures, vegetation composition and productivity, wetting and drying of soils, soil carbon balance, and wildlife and human activities. Permafrost degradation results in numerous types of thermokarst landforms, with a wide range of sizes, in response to topography, surficial geology, ground-ice morphology and abundance, hydrologic regimes and the degree of surface impacts (Jorgenson, 2013; Segal *et al*., 2016). Overall, the most prevalent thermokarst landforms include: deep and shallow lakes, drained lake basins, and bogs and fens in lowlands; thaw slumps and active-layer detachment slides on hillsides; and thermal erosion gullies and thermokarst pits and troughs associated with degrading ice wedges. In addition, coastal erosion degrades permafrost along the margins of the Arctic Ocean (Lantuit *et al*., 2012a). Below, we focus on landscape changes resulting from these processes that can be detected using remote sensing techniques. The broader patterns and processes related to thermokarst features were summarised by Kokelj and Jorgenson (2013).

Thermokarst lakes and drained lake basins are prominent in Arctic and boreal lowlands and have significant impacts on permafrost stability and biogeochemical cycling (Grosse *et al*., 2013; Walter-Anthony *et al*., 2014). Landsat imagery has been used in conjunction with DEMs to map the distribution of thermokarst lakes and drained lake basins in the Lena Delta (Morgenstern *et al*., 2011), the Seward Peninsula (Jones *et al*., 2011; Regmi *et al*., 2012) and northern Alaska (Wang *et al*., 2012). Other studies focused on multi-temporal Landsat data to track decadal-scale lake area changes. Bryksina and Polishchuk (2015) studied thermokarst lakes in West Siberia and found that new lake formation substantially exceeded lake losses due to drainage from 1973 to 2013. Karlsson *et al*. (2012) used multi-temporal analysis of lake areas in northwest Siberia from 1973 to 2009 and found substantial lake area fluctuations, with only one watershed having a long-term trend related to permafrost degradation. In Alaska, Chen *et al*. (2014) found that 350 of 2280 lakes shrank in the Yukon Flats, while 103 expanded, and that 81 per cent of lake area variability could be attributed to intra- and interannual variability in water balance and mean temperatures since snowmelt. Using 17 Landsat images, Olthof *et al*. (2015) mapped lake changes on the Tuktoyaktuk Peninsula to determine that net lake area increased by 40 km^2 over 26 years. Similarly, analysis of trends in multispectral band indices derived from temporally dense Landsat image stacks has been used to identify expanding and draining thermokarst lakes, as well as other land surface changes, in the Lena Delta over a 15 year period (Nitze and Grosse, 2016). Finer-scale aerial and satellite imagery also have been used to characterise changes in lakes and ponds at the landscape level, including for the Hudson Bay lowlands (Bouchard *et al*., 2014), the Barrow Peninsula (Andresen and Lougheed, 2015) and northern Quebec (Beck *et al*., 2015). Sannel and Kuhry (2011) manually delineated thermokarst lakes in a time series (1954–2007) of aerial photographs and Quickbird and Ikonos images for three boreal regions and found that lake area increased near Hudson Bay (0.9%/decade) and in West Siberia (0.04%/decade), but decreased in Sweden (-4.8%/decade), with shore fen infilling being a significant factor. In another type of remote sensing application, Lindgren *et al*. (2016) used low-altitude aerial photographs to map and quantify methane ebullition features in lake ice in interior Alaska and found that higher methane-seep densities occurred along lake shores with higher erosion rates, signalling a direct linkage between permafrost thaw along thermokarst lake margins and decomposition of previously frozen soil carbon.

Thermokarst bogs and fens have significant ecological consequences due to hydrologic reorganisation (Quinton *et al*., 2011; Jorgenson *et al*., 2013), thawing of old frozen soil carbon and sequestration of new carbon (Schuur *et al*., 2015), and shifts in vegetation from forests to wetlands (Sannel and Kuhry, 2011; Baltzer *et al*., 2014). Sannel and Kuhry (2011) found that shore fen infilling of thermokarst lakes affected 0.3 per cent of the map area per decade near Hudson Bay and 4.0 per cent of the area per decade in

northern Sweden. Quinton *et al*. (2011) analysed aerial photographs, Ikonos and LiDAR images from 1947 to 2008 for northwest Canada to determine that permafrost plateaus lost 38 per cent of their area over the period as thermokarst bogs and fens expanded. Lara *et al*. (2015) analysed aerial photographs and satellite imagery (1949–2011) to determine that 7 per cent of birch forests on permafrost plateaus were converted to thermokarst bogs and fens in central Alaska. Because these landforms are important to hydrologic regimes, Chasmer *et al*. (2014) used a decision-tree classification framework with airborne LiDAR and WorldView-2 imagery to better differentiate thermokarst bogs and fens from permafrost plateaus.

Thaw slumps and active-layer detachment slides are increasingly important landscape disturbances that affect the water quality of nearby lakes and streams (Kokelj *et al*., 2013; Segal *et al*., 2016), vegetation and soils (Lantuit *et al*., 2012b; Khomutov and Leibman, 2014), and trace gases (Abbott and Jones, 2015). Brooker *et al*. (2014) performed tasselled cap analyses on 18 Landsat images (1988–2011) to map thaw slumps by activity level, calculate growth rates and evaluate vegetation colonisation patterns. Balser *et al*. (2014) used SAR and optical imagery to examine thaw slump initiation between 1997 and 2010 and found that 80 per cent of the slumps appeared during summers 2004 and 2005 in response to unusually high air temperatures and early snowmelt in 2004. By manually interpreting Ikonos imagery, Swanson (2013) identified 2200 active-layer detachment slides and ~ 700 thaw slumps in northwestern. Swanson (2012) also has been monitoring 26 thaw slumps using handheld aerial photographs taken from a helicopter to create photogrammetric DEMs and found areal changes of 0 to 1 ha, with the most active slump losing 30 000 m^3 between 2010 and 2011. Kokelj *et al*. (2013) used Quickbird and SPOT images (2007–10) to manually map 60+ active thaw slumps on Peel Plateau, Northwest Territories, with nine 'megaslumps' > 5 ha. A megaslump in northwest Alaska monitored using terrestrial laser scanning mobilised more than 500 000 m^3 of ice and sediment, and expanded at a rate of 20 m/yr (Barnhart and Crosby, 2013). Khomutov and Leibman (2014) made a geomorphological map for a portion of the Yamal Peninsula and showed that thaw slumps and detachment slides affected ~ 20 per cent of the landscape. Lacelle *et al*. (2010) analysed aerial photographs (1950 – 2004) for thaw slump occurrence in the Richardson Mountains and found that new thaw slump initiation increased from 0.35 slumps/yr during 1954–71 to 0.68 slumps/yr during 1985–2004. Short *et al*. (2011) used InSAR data-sets derived from TerraSAR-X, RADARSAT-2 and ALOS-Phased Array Type L-band Synthetic Aperature Radar to measure surface displacement in thaw slumps on Herschel Island, northwest Canada, but concluded that the technique had serious limitations. Rudy *et al*. (2013) successfully used NDVI changes based on multi-temporal IKONOS satellite imagery to detect active-layer detachment slides, with more success with destructive elongate forms than with better-vegetated compact forms.

Thermal erosion gullies and valleys are indicative of hydrologic changes associated with degrading ice-rich permafrost terrain (Morgenstern, 2012; Godin *et al*., 2014), and are important pathways for export of carbon and nutrients from thawing permafrost (Abbott and Jones, 2015). Godin *et al*. (2014) used aerial photographs and very high-resolution satellite images to map the expansion of 35 degrading ice-wedge gullies on Bylot Island from 1972 to 2013; the gullies covered 158 000 m^2 by 2013, breached adjacent low-centred polygons and channellised hydrologic flow paths. Belshe *et al*. (2013) used Ikonos images and differential GPS to characterise small thermokarst landforms and found that they covered 12 per cent of an alpine hillslope in interior Alaska, even though gullies averaged ~ 1 m in width. In north Siberia, Morgenstern (2012) mapped the distribution of large thermal erosion gullies and valleys using high to medium-resolution multi-sensor optical imagery and DEMs across three regions with yedoma permafrost and found maximum valley depths of 35 m and valley densities from 0.9 to 1.8 km/km^2. These features remain understudied.

Thermokarst pits and troughs associated with degrading ice-wedge polygonal networks affect water movement in low-gradient watersheds, energy fluxes and soil temperatures, soil organic accumulation, and vegetation composition and structure (Jorgenson *et al*., 2015). Ice wedges may occupy 5–25 per cent of the volume of the upper 3 m of permafrost depending on geology and age, and occupy 30–80 per cent of the volume in Pleistocene-age yedoma (Kanevskiy *et al*., 2013; Ulrich *et al*., 2014). Jorgenson *et al*. (2015c) manually delineated water-filled thermokarst troughs near Prudhoe Bay on a time series of eight aerial photographs (1949–2012) and found that troughs increased from 0.9 per cent to 7.5 per cent over the period and attributed the degradation to extremely warm summers in 1989 and 1998. Steedman *et al*. (2016) manually mapped water-filled troughs on 1972 and 2004 aerial photographs at 237 locations in the Tuktoyaktuk Coastlands and found that water area increased only 0.1 per cent, although the prevalence of high-centred polygons indicated that previous degradation was extensive. Jones *et al*. (2013a) used repeat LiDAR (2006, 2010) to identify > 300 thermokarst pits that subsided as a result of storm surge flooding along the Beaufort coast. Repeat LiDAR also was used by Jones *et al*. (2015) to show that thaw subsidence affected 34 per cent of the area 7 years after a tundra fire in northern Alaska, mostly associated with ice-wedge degradation (Figure 3). Necsoiu *et al*. (2013) used orthorectified aerial images for the Kobuk region in Alaska to determine that water-filled troughs from ice-wedge degradation covered 3 per cent of the 2005 images, but were absent in 1951.

Coastal erosion and storm surge flooding along the margins of the Arctic Ocean endanger human settlements and infrastructure, alter fish and wildlife habitats, affect permafrost stability and contribute to transfer of terrestrial organic carbon to the marine ecosystem (Overduin *et al*., 2014). Because permafrost coasts comprise ~ 30 per cent

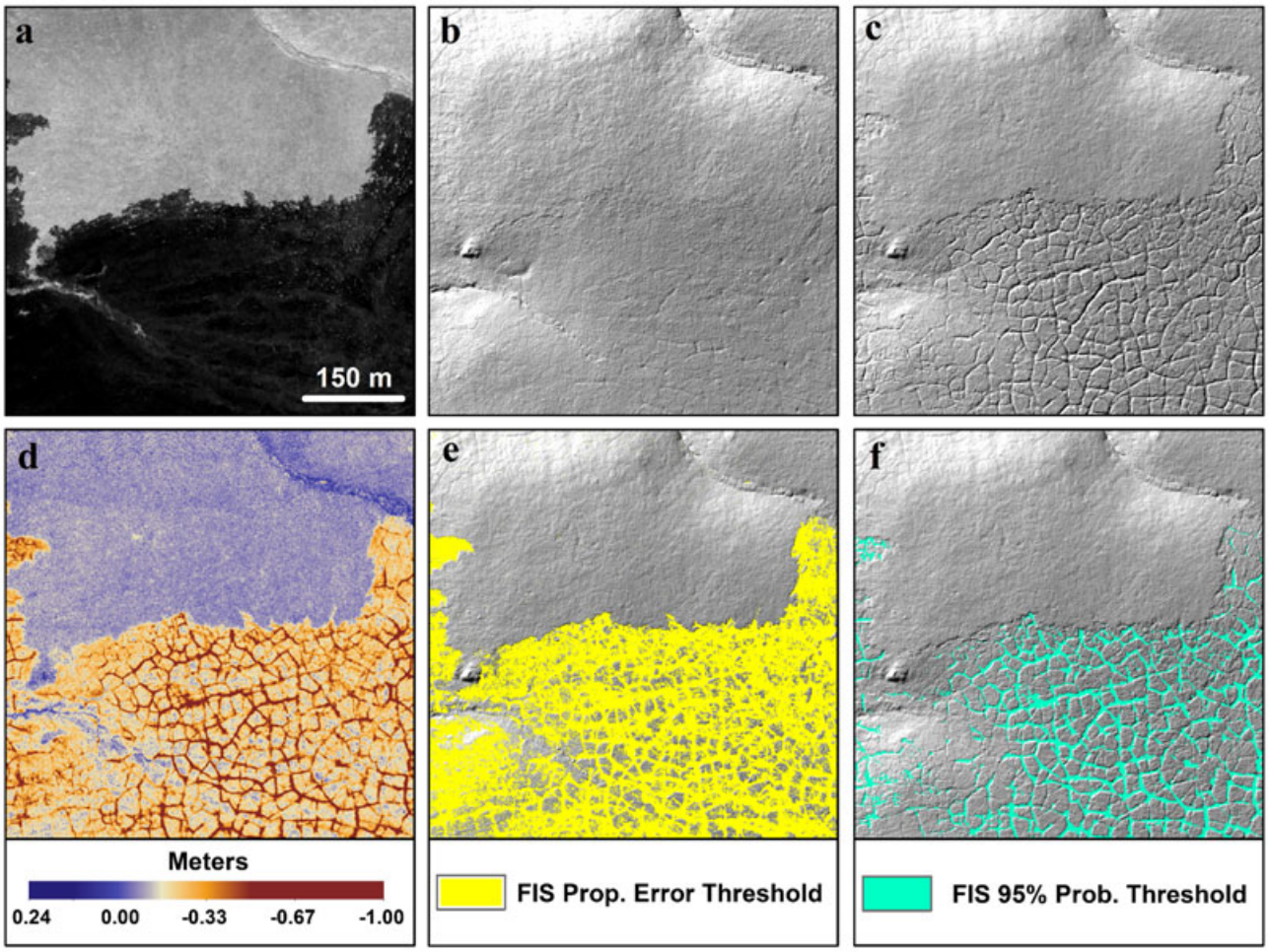

Figure 3 Detection of subsidence associated with thawing ice wedges in burned tundra in northern Alaska using multi-temporal light detection and ranging (LiDAR) (from Jones *et al*., 2015). (a) A Quickbird image from 5 July 2008, the year following the fire, differentiating burned (dark) and unburned (light) tundra. Hillshade images of (b) 2009 and (c) 2014 1 m resolution LiDAR. (d) Raw differential digital terrain model (DTM) created by differencing the 2009 and 2014 DTMs. Detectable change was determined using (e) the FIS propagation of errors threshold (> ~ 0.2 m) and (f) the FIS 95 per cent probability threshold (> ~ 0.5 m).

of the world's coastline, a large international effort by the Arctic Coastal Dynamics programme compiled data on permafrost characteristics and shoreline changes for 101 447 km of coastline (Lantuit *et al*., 2012a), and determined that the mean annual erosion rate was 0.5 m/yr. More recently, Gibbs and Richmond (2015) visually derived land-water interface positions for the Beaufort and Chukchi coastlines in northern Alaska from historical and recent (1997–2012) aerial photographs, Quickbird and Spot imagery, and LiDAR to determine a mean annual erosion rate of 1.4 m/yr (range -18.6 to 10.9 m/yr, with loss negative). Obu *et al*. (2016) investigated permafrost coastal erosion along the Canadian Beaufort Sea with repeat LiDAR and found that the volume of sediments released by thaw slumps was important to shoreline erosion and aggradation rates over annual (2012–13) timescales. Günther *et al*. (2013) used CORONA (1965) and recent imagery (ALOS Panchromatic Remote Sensing Instrument for Stereo Mapping, KOMPSAT-2, RapidEye and GeoEye, 2007–11) to manually map three coastal segments (75–95 km) in the Laptev Sea region and found that mean annual erosion rates were higher in recent years (-5.3 m/yr) than the long-term mean (-2.2 m/yr). The acceleration in erosion rates in the Arctic is attributed to the increased open-water season, fetch and wave energy resulting from sea ice loss (Vermaire *et al*., 2013). Coastal flooding can also cause significant change in low-lying coastal areas. Lantz *et al*. (2015) analysed Landsat-derived NDVI data (1986 and 2011) for the Mackenzie Delta to detect impacts from a 1999 storm flood and found that vegetation was damaged on 31 204 ha of the outer delta and roughly two-thirds of the affected area subsequently recovered. Terenzi *et al*. (2014) used Radarsat-1, MODIS and Ikonos imagery to map the extent of storm flooding on the Yukon-Kuskokwim Delta and found that the maximum inland extent of flooding from three large storms varied from 27.4 to 32.3 km.

SYNTHESIS AND CONCLUSION

Tremendous progress has been made during the last 5 years in using remote sensing to quantify the state and changes in permafrost-affected landscapes and to assess the complexity of local to regional differences and variability over time. In many cases, the results show strong trends in landscape characteristics as they respond to amplification of global warming in the Arctic. Analyses using low to moderate-resolution imagery have revealed increasing LSTs and vegetation biomass, and decreasing duration of snow cover, influenced by the rapidly declining extent of sea ice. These hemispheric-scale studies reveal substantial regional differences and provide long temporal records, but lack the ground resolution necessary to capture the spatial complexity of landscape responses, especially those related to permafrost processes. Local-scale studies involving high-resolution imagery also have found consistent increases in vegetation biomass and shrub expansion in the Arctic, although there appear to be strong landscape-level controls on where increases (and decreases) occur. The extent of permafrost degradation and associated thermokarst landforms are increasing, with many studies noting acceleration during the last decade or two. Even under colder Arctic conditions, thawing of ground ice near the surface is leading to collapsing topography. Fire frequency and extent, especially large fires, are increasing in boreal regions leading to a shift toward deciduous forests, and there have been recent notable fires in the Arctic. Less clear are trends in surface water and land cover. Both regional and landscape-level analyses show inconsistent trends in surface water extent, with high seasonal, annual and regional variability, due in part to differences in methods and spatial scales. The surface water analyses are revealing complicated interactions involving water increases from permafrost degradation, lake initiation and shoreline erosion; decreases from lake drainage and shoreline paludification; and multi-year bi-directional fluctuations due to water balance changes. Similarly, overall trends in high-resolution land cover in permafrost regions remain elusive due to differences in classification, imagery types, processing techniques, and the role of disturbance and succession in complicating long-term trends.

Recent progress in remote sensing has been facilitated by expanding sensor capabilities across the electromagnetic spectrum, higher-resolution imagery, new image processing techniques, enhanced public access to data and increasingly long image archives now covering multiple decades. Particularly notable progress has been made using multi-sensor data fusion and multivariate analysis to assess interacting biophysical factors to understand causative factors better and by incorporating remote sensing time-series products as inputs to process-based models. Emerging remote sensing methods that appear especially promising include: repeat LiDAR, InSAR and airborne geophysics for detecting topographic and subsurface changes; and high-temporal trend analysis of surface characteristics at high spatial resolution.

Some important challenges remain, however, in using remote sensing to understand landscape change, including better mapping of ground ice, snow properties, land cover classes relevant to permafrost characteristics, and more comprehensive assessments of thermokarst (especially smaller-scale features). There is an increasing need to integrate and fuse independent data-sets involving multiple landscape components into the remote sensing analyses to better understand the broad-scale drivers and constraints on landscape change. While there has been tremendous progress in the integration of global, low-resolution data-sets, it has been more difficult to integrate and synthesise the increasing numbers of localised, high-resolution studies into hemispheric trends. Thus, there need to be coordinated efforts to use high-resolution imagery in systematic and well-distributed analyses of local changes within broader regional sampling frameworks. As can be seen from this review, we are accumulating evidence of landscape changes from many sites, with some studies incorporating sampling from dozens of sites, but it is difficult to synthesise these trends without a more standardised and systematically distributed effort. Furthermore, there needs to be increased use of high-resolution mapping to evaluate patterns and trends in coarse-scale mapping.

Because permafrost and ground ice are so fundamental to the evolution of northern landscapes, with global implications, it is urgent to further improve remote sensing capabilities and techniques for assessing permafrost distribution, thermokarst and surface deformation, ground-ice distribution and biophysical interactions (e.g. surface water, soil moisture and organic material, vegetation) that provide feedbacks to permafrost stability. There has been substantial progress in incorporating remote sensing products (e.g. LSTs) into mapping and modelling of permafrost distribution, especially at landscape scales, yet little progress has been made in remote sensing of ground ice. Increased availability and use of very high-resolution imagery are needed to better understand ground ice and permafrost dynamics, because permafrost degradation occurs only at the metre scale over years. Similarly, increased acquisition and availability of IfSAR, LiDAR and SfM-derived topography will be fundamental for better quantification of thermokarst. Finally, remote sensing of long-term trends in land surface properties, such as LSTs, snow cover, surface water, soil moisture and vegetation, as well as of disturbances and successional trajectories related to fire and thermokarst, will provide valuable data for assessing factors affecting permafrost degradation and stability under current and future climates.

ACKNOWLEDGEMENTS

This review was supported by funding for Jorgenson from the National Science Foundation (ARC 1023623) and for Grosse from the European Research Commission (ERC 338335). The authors do not have any conflicts of interest associated with this review.

REFERENCES

Abbott BW, Jones JB. 2015. Permafrost collapse alters soil carbon stocks, respiration, CH_4, and N_2O in upland tundra. *Global Change Biology* **21**: 4570–4587.

Andresen CG, Lougheed VL. 2015. Disappearing Arctic tundra ponds: Fine-scale analysis of surface hydrology in drained thaw lake basins over a 65 year period (1948–2013). *Journal of Geophysical Research: Biogeosciences* **120**: 1–14.

Arp CD, Jones BM, Grosse G. 2013. Recent lake ice-out phenology within and among lake districts of Alaska, U.S.A. *Limnology and Oceanography* **58**: 2013–2028.

Baird RA, Verbyla D, Hollingsworth TN. 2012. Browning of the landscape of interior Alaska based on 1986–2009 Landsat sensor NDVI. *Canadian Journal of Forest Research* **42**: 1371–1382.

Balser AW, Jones JB, Gens R. 2014. Timing of retrogressive thaw slump initiation in the Noatak Basin, northwest Alaska, USA. *Journal of Geophysical Research: Earth Surface* **119**: 1106–1120.

Baltzer JL, Veness T, Chasmer LE, Sniderhan AE, Quinton WL. 2014. Forests on thawing permafrost: fragmentation, edge effects, and net forest loss. *Global Change Biology* **20**: 824–834.

Barnhart TB, Crosby BT. 2013. Comparing two methods of surface change detection on an evolving thermokarst using high-temporal-frequency terrestrial laser scanning, Selawik River, Alaska. *Remote Sensing* **5**: 2813–2837.

Barrett K, McGuire AD, Hoy EE, Kasischke E. 2011. Potential shifts in dominant forest cover in interior Alaska driven by variations in fire severity. *Ecological Applications* **21**: 2380–2396.

Beck I, Ludwig R, Bernier M, Lévesque E, Boike J. 2015. Assessing permafrost degradation and land cover changes (1986–2009) using remote sensing data over Umiujaq, Sub-Arctic Québec. *Permafrost and Periglacial Processes* **26**: 129–141.

Beck PSA, Goetz SJ. 2011. Satellite observations of high northern latitude vegetation productivity changes between 1982 and 2008: ecological variability and regional differences. *Environmental Research Letters* **6**: 045501.

Beck PSA, Goetz SJ, Mack MC, Alexander HD, Jin Y, Randerson JT, Loranty MM. 2011. The impacts and implications of an intensifying fire regime on Alaskan boreal forest composition and albedo. *Global Change Biology* **17**: 2853–2866.

Belshe EF, Schuur EAG, Grosse G. 2013. Quantification of upland thermokarst features with high resolution remote sensing. *Environmental Research Letters* **8**: 035016.

Bhatt US, Walker DA, Raynolds MK, Bieniek PA, Epstein HE, Comiso JC, Pinzon JE, Tucker CJ, Polyakov IV. 2013. Recent declines in warming and arctic vegetation greening trends over pan-Arctic tundra. *Remote Sensing* **5**: 4229–4254.

Blok D, Schaepman-Strub G, Bartholomeus H, Heijmans M, Maximov TC, Berendse F. 2011. The response of Arctic vegetation to the summer climate: relation between shrub cover, NDVI, surface albedo and temperature. *Environmental Research Letters* **6**: 035502.

Bonnaventure PP, Lewkowicz AG, Kremer M, Sawada MC. 2012. A permafrost probability model for the southern Yukon and northern British Columbia, Canada. *Permafrost and Periglacial Processes* **23**: 52–68.

Bouchard F, Francus P, Pienitz R, Laurion I, Feyte S. 2014. Subarctic thermokarst ponds: investigating recent landscape evolution and sediment dynamics in thawed permafrost of Northern Québec (Canada). *Arctic, Antarctic, and Alpine Research* **46**: 251–271.

Brooker A, Fraser RH, Olthof I, Kokelj SV, Lacelle D. 2014. Mapping the activity and evolution of retrogressive thaw slumps by tasselled cap trend analysis of a Landsat satellite image stack. *Permafrost and Periglacial Processes* **25**: 243–256.

Brown R, Derksen C. 2013. Is Eurasian October snow cover extent increasing? *Environmental Research Letters* **8**: 024006.

Brown RD, Robinson DA. 2011. Northern Hemisphere spring snow cover variability and change over 1922–2010 including an assessment of uncertainty. *The Cryosphere* **5**: 219–229.

Bryksina NA, Polishchuk YM. 2015. Analysis of changes in the number of thermokarst lakes in permafrost of West Siberia on the basis of satellite images. *Earth's Cryosphere* **2**: 114–120.

Carroll ML, Townshend JRG, DiMiceli CM, Loboda T, Sohlberg RA. 2011. Shrinking lakes of the Arctic: spatial relationships and trajectory of change. *Geophysical Research Letters* **38**: L20406.

Chapin FS III, Oswood MW, Van Cleve K, Viereck LA, Verbyla DL. 2006. Alaska's Changing Boreal Forest. Oxford University Press: New York.

Chasmer L, Hopkinson C, Veness T, Quinton W, Baltzer J. 2014. A decision-tree classification for low-lying complex land cover types within the zone of discontinuous permafrost. *Remote Sensing of Environment* **143**: 73–84.

Chen F, Lin H, Zhou W, Hong T, Wang G. 2013. Surface deformation detected by ALOS PALSAR small baseline SAR interferometry over permafrost environment of Beiluhe section, Tibet Plateau, China. *Remote Sensing of Environment* **138**: 10–18.

Chen M, Rowland JC, Wilson CJ, Altmann GL, Brumby SP. 2014. Temporal and spatial pattern of thermokarst lake area changes at Yukon Flats, Alaska. *Hydrological Processes* **28**: 837–852.

Ducks Unlimited. 2013. North Slope Science Initiative Landcover Mapping Summary Report Rancho Cordova, CA; 51pp.

Epstein HE, Myers-Smith I, Walker DA. 2013. Recent dynamics of arctic and sub-arctic vegetation. *Environmental Research Letters* **8**: 015040.

Fraser R, Olthof I, Kokelj S, Lantz T, Lacelle D, Brooker A, Wolfe S, Schwarz S. 2014. Detecting landscape changes in high latitude environments using Landsat trend analysis: 1. visualization. *Remote Sensing* **6**: 11533–11557.

Fraser RH, Olthof I, Maloley M, Fernandes R, Prevost C, van der Sluijs J. 2015. UAV photogrammetry for mapping and monitoring of northern permafrost landscapes. *International Archives of the Photogrammetry. Remote Sensing and Spatial Information Sciences* **XL-1/W4**: 361–361.

Frost GV, Epstein HE. 2014. Tall shrub and tree expansion in Siberian tundra ecotones since the 1960s. *Global Change Biology* **20**: 1264–1277CITED incorrectly in text.

Gibbs AE, Richmond BM. 2015. National Assessment of Shoreline Change–Historical Shoreline Change along the North Coast of Alaska, U.S.–Canadian Border to Icy CapeU.S. Geological Survey Open–File Report 2015–1048.

Godin E, Fortier D, Coulombe S. 2014. Effects of thermo-erosion gullying on hydrologic flow networks, discharge and soil loss. *Environmental Research Letters* **9**: 105010.

Gogineni P, Romanovsky V, Cherry J, Duguay C, Goetz S, Jorgenson MT, Moghaddami M. 2014. Opportunities to use Remote Sensing in Understanding Permafrost and Related Ecological Characteristics: Report of a Workshop. The National Academies Press: Washington, DC.

Grosse G, Harden J, Turetsky M, McGuire DA, Camill P, Tarnocai C, Frolking S, Schuur EA, Jorgenson T, Marchenko S, Romanovsky V, Wickland KP, French NH, Waldrop M, Bourgeau-Chavez L, Striegl RG. 2011a. Vulnerability of high-latitude soil organic carbon in North America to disturbance. *Journal of Geophysical Research* **116**: G00K06.

Grosse G, Romanovsky V, Jorgenson T, Anthony KW, Brown J. 2011b. Vulnerability and feedbacks of permafrost to climate change. *Eos, Transactions American Geophysical Union* **92**: 73–80.

Grosse G, Jones B, Arp C. 2013. Thermokarst lakes, drainage, and drained basins. In Treatise on Geomorphology, John F, Shroder JF (eds). Academic Press; 325–353.

Grunblatt J, Atwood D. 2014. Mapping lakes for winter liquid water availability using SAR on the North Slope of Alaska. *International Journal of Applied Earth Observation and Geoinformation* **27**: 63–69.

Günther F, Overduin PP, Sandakov AV, Grosse G, Grigoriev MN. 2013. Short- and long-term thermo-erosion of ice-rich permafrost coasts in the Laptev Sea region. *Biogeosciences* **10**: 4297–4318.

Günther F, Overduin PP, Yakshina IA, Opel T, Baranskaya AV, Grigoriev MN. 2015. Observing Muostakh disappear: permafrost thaw subsidence and erosion of a ground-ice-rich island in response to arctic summer warming and sea ice reduction. *The Cryosphere* **9**: 151–178.

Hancock S, Baxter R, Evans J, Huntley B. 2013. Evaluating global snow water equivalent products for testing land surface models. *Remote Sensing of Environment* **128**: 107–117.

Hinkel KM, Lin Z, Sheng Y, Lyons EA. 2012. Regional lake ice meltout patterns near Barrow, Alaska. *Polar Geography* **35**: 1–18.

Hubbard SS, Gangodagamage C, Dafflon B, Wainwright H, Peterson J, Gusmeroli A, Ulrich C, Wu Y, Wilson CJ, Rowland JC, Tweedie CE, Wullschleger SD. 2013. Quantifying and relating land-surface and subsurface variability in permafrost environments using LiDAR and surface geophysical datasets. *Hydrogeology Journal* **21**: 149–169.

Jafarov EE, Marchenko SS, Romanovsky VE. 2012. Numerical modeling of permafrost dynamics in Alaska using a high spatial resolution dataset. *The Cryosphere* **6**: 613–624.

Jafarov EE, Romanovsky VE, Genet H, McGuire AD, Marchenko SS. 2013. The effects of fire on the thermal stability of permafrost in lowland and upland black spruce forests of interior Alaska in a changing climate. *Environmental Research Letters* **8**: 035030.

Joly K, Klein DR, Verbyla DL, Rupp TS, Chapin FS III. 2011. Linkages between large-scale climate patterns and the dynamics of Arctic caribou populations. *Ecography* **34**: 345–352.

Jones BM, Grosse G, Arp CD, Jones MC, Walter Anthony KM, Romanovsky VE. 2011. Modern thermokarst lake dynamics in the continuous permafrost zone, northern Seward Peninsula, Alaska. *Journal of Geophysical Research: Biogeosciences* **116**: G00M03.

Jones BM, Stoker JM, Gibbs AE, Grosse G, Romanovsky VE, Douglas TA, Kinsman NEM, Richmond BM. 2013a. Quantifying landscape change in an arctic coastal lowland using repeat airborne LiDAR. *Environmental Research Letters* **8**: 045025.

Jones BM, Breen AL, Gaglioti BV, Mann DH, Rocha AV, Grosse G, Walker DA. 2013b. Identification of unrecognized tundra fire events on the North Slope of Alaska. *Journal of Geophysical Research: Biogeosciences* **118**: 1334–1344.

Jones BM, Grosse G, Arp CD, Liu L, Miller EA, Hayes DJ, Larsen C. 2015. Recent arctic tundra fire initiates widespread thermokarst development. *Scientific Reports* **5**: 15865.

Jorgenson MT. 2013. Thermokarst terrains. In Treatise on Geomorphology, Schroeder J, Giardino R, Harbor J (eds). Academic Press: San Diego; 313–324.

Jorgenson MT, Harden J, Kanevskiy M, O'Donnel J, Wickland K, Ewing S, Manies K, Zhuang Q, Shur Y, Striegl R, Koch J. 2013. Reorganization of vegetation, hydrology and soil carbon after permafrost degradation across heterogeneous boreal landscapes. *Environmental Research Letters* **8**: 035017.

Jorgenson MT, Marcot BG, Swanson DK, Jorgenson JC, DeGange AR. 2015a. Projected changes in diverse ecosystems from climate warming and biophysical drivers in northwest Alaska. *Climatic Change* **130**: 131–144.

Jorgenson MT, Kanevskiy M, Shur Y, Grunblatt J, Ping CL, Michaelson G. 2015b. Permafrost database development, characterization, and mapping for northern Alaska. Arctic Landscape Conservation Cooperative, Fairbanks, AK. https://catalog.data.gov/dataset/permafrost-soils-database-for-northern-alaska-2014

Jorgenson MT, Kanevksiy MZ, Shur Y, Wickland K, Nossov DR, Moskalenko NG, Koch J, Striegl R. 2015c. Role of ground-ice dynamics and ecological feedbacks in ice-wedge degradation and stabilization. *Journal of Geophysical Research - Earth Surface* **120**: 2280–2297.

Kääb A, Girod L, Berthling I. 2014. Surface kinematics of periglacial sorted circles using structure-from-motion technology. *The Cryosphere* **8**: 1041–1056.

Kanevskiy M, Shur Y, Jorgenson MT, Ping CL, Michaelson GJ, Fortier D, Stephani E, Dillon M, Tumskoy VE. 2013. Ground ice in the upper permafrost of the Beaufort Sea coast of Alaska. *Cold Regions Science and Technology* **85**: 56–70.

Karlsson JM, Lyon SW, Destouni G. 2012. Thermokarst lake, hydrological flow and water balance indicators of permafrost change in Western Siberia. *Journal of Hydrology* **464**: 459–466.

Kasischke ES, Verbyla DL, Rupp TS, McGuire AD, Murphy KA, Jandt R, Barnes JL, Hoy EE, Duffy PA, Calef M, Turetsky MR. 2010. Alaska's changing fire regime — implications for the vulnerability of its boreal forests. *Canadian Journal of Forest Research* **40**: 1313–1324.

Khomutov A, Leibman M. 2014. Assessment of landslide hazards in a typical tundra of central Yamal, Russia. In Landslides in Cold Regions in the Context of Climate Change, Shan W et al. (eds). Springer International Publishing: Switzerland; 271–290.

Kizyakov AI, Sonyushkin AV, Leibman MO, Zimin MV, Khomutov AV. 2015. Geomorphological conditions of the gas-emission crater and its dynamics in Central Yamal. *Earth's Cryosphere* **2**: 15–25.

Kokelj SV, Jorgenson MT. 2013. Advances in Thermokarst Research. *Permafrost and Periglacial Processes* **24**: 108–119.

Kokelj SV, Lacelle D, Lantz TC, Tunnicliffe J, Malone L, Clark ID, Chin KS. 2013. Thawing of massive ground ice in mega slumps drives increases in stream sediment and solute flux across a range of watershed scales. *Journal of Geophysical Research, Earth Surface* **118**: 681–692.

Kumpula T, Forbes BC, Stammler F, Meschtyb N. 2012. Dynamics of a coupled system: multi-resolution remote sensing in assessing social-ecological responses during 25 years of gas field development in Arctic Russia. *Remote Sensing* **4**: 1046–1068 Check Citation in text.

Lacelle D, Bjornson J, Lauriol B. 2010. Climatic and geomorphic factors affecting contemporary (1950-2004) activity of retrogressive thaw slumps on the Aklavik Plateau, Richardson Mountains, NWT, Canada. *Permafrost and Periglacial Processes* **21**: 1–15.

Langer M, Westermann S, Heikenfeld M, Dorn W, Boike J. 2013. Satellite-based modeling of permafrost temperatures in a tundra lowland landscape. *Remote Sensing of Environment* **135**: 12–24.

Lantuit H, Overduin PP, Couture NJ, Wetterich S, Aré F, Atkinson D, Brown J, Cherkashov G, Drozdov D, Forbes DL, Graves-Gaylord A, Grigoriev M, Hubberten H-W, Jordan J, Jorgenson T, Ødegård RS, Ogorodov S, Pollard WH, Rachold V, Sedenko D, Solomon S, Steenhuisen F, Streletskaya I, Vasiliev A. 2012a. The Arctic Coastal Dynamics Database: A New Classification Scheme and Statistics on Arctic Permafrost Coastlines. *Estuaries and Coasts* **35**: 383–400.

Lantuit H, Pollard WH, Couture N, Fritz M, Schirrmeister L, Meyer H, Hubberten HW. 2012b. Modern and Late Holocene

Retrogressive Thaw Slump Activity on the Yukon Coastal Plain and Herschel Island, Yukon Territory, Canada. *Permafrost and Periglacial Processes* **23**: 39–51.

Lantz TC, Turner KW. 2015. Changes in lake area in response to thermokarst processes and climate in Old Crow Flats, Yukon. *Journal of Geophysical Research, Biogeosciences* **120**: 513–524.

Lantz TC, Marsh P, Kokelj SV. 2013. Recent shrub proliferation in the Mackenzie Delta uplands and microclimatic implications. *Ecosystems* **16**: 47–59.

Lantz TC, Kokelj SV, Frazer RH. 2015. Ecological recovery in an Arctic delta following widespread saline incursion. *Ecological Applications* **25**: 172–185.

Lara MJ, Genet H, McGuire AD, Euskirchen ES, Zhang Y, Brown D, Jorgenson MT, Romanovsky VE, Breen A, Lee H, Bolton WR. 2015. Thermokarst rates intensify due to climate change and forest fragmentation in an Alaskan boreal forest lowland. *Global Change Biology* **22**: 816–829.

Latifovic R, Fernandes R, Pouliot D, Olthof I. 2014. Characterization and Monitoring Change of Canada's Land Surface. Natural Resources Canada. http://www.nrcan.gc.ca/

Lawrence DM, Swenson SC. 2011. Permafrost response to increasing Arctic shrub abundance depends on the relative influence of shrubs on local soil cooling versus large-scale climate warming. *Environmental Research Letters* **6**: 045504.

Li Z, Zhao R, Hu J, Wen L, Feng G, Zhang Z, Wang Q. 2015. InSAR analysis of surface deformation over permafrost to estimate active layer thickness based on one-dimensional heat transfer model of soils. *Scientific Reports* **5**: 15542.

Lin DH, Johnson DR, Andresen C, Tweedie CE. 2012. High spatial resolution decade-time scale land cover change at multiple locations in the Beringian Arctic (1948–2000s). *Environmental Research Letters* **7**: 025502.

Lindgren PR, Grosse G, Walter Anthony KM, Meyer FJ. 2016. Detection and spatiotemporal analysis of methane ebullition on thermokarst lake ice using high-resolution optical aerial imagery. *Biogeosciences* **13**: 27–44.

Lindsay C, Zhu J, Miller AE, Kirchner P, Wilson TL. 2015. Deriving snow cover metrics for Alaska from MODIS. *Remote Sensing* **7**: 12961–12985.

Liu L, Schaefer K, Zhang T, Wahr J. 2012. Estimating 1992–2000 average active layer thickness on the Alaskan North Slope from remotely sensed surface subsidence. *Journal of Geophysical Research* **117**: F01005.

Liu L, Jafarov EE, Schaefer KM, Jones BM, Zebker HA, Williams CA, Rogan J, Zhang T. 2014. InSAR detects increase in surface subsidence caused by an Arctic tundra fire. *Geophysical Research Letters* **41**: 3906–3913.

Loranty MM, Goetz SJ. 2012. Shrub expansion and climate feedbacks in Arctic tundra. *Environmental Research Letters* **7**: 011005.

Loranty MM, Natali SM, Berner LT, Goetz SJ, Holmes RM, Davydov SP, Zimov NS, Zimov SA. 2014. Siberian tundra ecosystem vegetation and carbon stocks four decades after wildfire. *Journal of Geophysical Research: Biogeosciences* **119**: 2144–2154.

Lu X, Zhuang Q. 2011. Areal changes of land ecosystems in the Alaskan Yukon River Basin from 1984 to 2008. *Environmental Research Letters* **6**: 034012.

Macander MJ, Swingley CS, Joly K, Raynolds MK. 2015. Landsat-based snow persistence map for northwest Alaska. *Remote Sensing of Environment* **163**: 23–31.

Minsley BJ, Abraham JD, Smith BD, Cannia JC, Voss CI, Jorgenson MT, Walvoord MA, Wylie BK, Anderson L, Ball LB, Deszcz-Pan M, Wellman TP, Ager TA. 2012. Airborne electromagnetic imaging of discontinuous permafrost. *Geophysical Research Letters* **39**: L02503.

Moore RD, Fleming SW, Menounos B, Wheate R, Fountain A, Stahl K, Holm K, Jakob M. 2009. Glacier change in western North America: influences on hydrology, geomorphic hazards and water quality. *Hydrological Processes* **23**: 42–61.

Morgenstern A. 2012. Thermokarst and thermal erosion: Degradation of Siberian ice-rich permafrost. PhD thesis, University of Potsdam.

Morgenstern A, Grosse G, Günther F, Fedorova IV, Schirrmeister L. 2011. Spatial analyses of thermokarst lakes and basins in Yedoma landscapes of the Lena Delta. *The Cryosphere* **5**: 849–867.

Muskett R. 2012. Multi-satellite and sensor derived trends and variation of snow water equivalent on the high-latitudes of the Northern Hemisphere. *International Journal of Geosciences* **3**: 1–13.

Muster S, Heim B, Abnizova A, Boike J. 2013. Water body distributions across scales: a remote sensing based comparison of three Arctic tundra wetlands. *Remote Sensing* **5**: 1498–1523.

Myers-Smith IH, Hik DS. 2013. Shrub canopies influence soil temperature but no nutrient dynamics: An experimental test of tundra snow-shrub interactions. *Ecology and Evolution* **3**: 3683–3700.

Myers-Smith IH, Forbes BC, Wilmking M, Hallinger M, Lantz T, Blok D, Tape KD, Macias-Fauria M, Sass-Klaassen U, Esther L, Ropars P, Hermanutz L, Trant A, Siegwart Collier L, Weijers S, Rozema J, Rayback SA, Schmidt NM, Schaepman-Strub G, Wipf S, Rixen C, Venn S, Goetz S, Andreu-Hayles L, Elmendorf S, Ravolainen V, Welker J, Grogan P, Epstein HE, Hik DS. 2011. Shrub expansion in tundra ecosystems: Dynamics, impacts and research priorities. *Environmental Research Letters* **6**: 045509.

Naito AT, Cairns DM. 2015. Patterns of shrub expansion in Alaskan arctic river corridors suggest phase transition. *Ecology and Evolution* **5**: 87–101.

Necsoiu M, Dinwiddie CL, Walter GR, Larsen A, Stothoff SA. 2013. Multi-temporal image analysis of historical aerial photographs and recent satellite imagery reveals evolution of water body surface area and polygonal terrain morphology in Kobuk Valley National Park, Alaska. *Environmental Research Letters* **8**: 025007.

Nitze I, Grosse G. 2016. Detection of landscape dynamics in the Arctic Lena Delta with temporally dense Landsat time-series stacks. *Remote Sensing of Environment* **181**: 27–41.

Nolan M, Larsen CF, Sturm M. 2015. Mapping snow depth from manned aircraft on landscape scales at centimeter resolution using structure-from-motion photogrammetry. *The Cryosphere* **9**: 1445–1463.

Obu J, Lantuit H, Grosse G, Günther F, Sachs T, Helm V, Fritz M. 2016. Coastal erosion and mass wasting along the Canadian Beaufort Sea based on annual airborne LiDAR elevation data. *Geomorphology* DOI:10.1016/j.geomorph.2016.02.014

Olthof I, Latifovic R, Pouliot D. 2009. Development of a circa 2000 land cover map of northern Canada at 30 m resolution from Landsat. *Canadian Journal of Remote Sensing* **35**: 152–165.

Olthof I, Fraser RH, Schmitt C. 2015. Landsat-based mapping of thermokarst lake dynamics on the Tuktoyaktuk Coastal Plain, Northwest Territories, Canada since 1985. *Remote Sensing of Environment* **168**: 194–204.

Overduin PP, Strzelecki MC, Grigoriev MN, Couture N, Lantuit H, St-Hilaire-Gravel D, Günther F, Wetterich S. 2014. Coastal changes in the Arctic. *Geological Society, London, Special Publications* **388**: 103–129.

Paine JG, Andrews JR, Saylam K, Tremblay TA, Averett AR, Caudle TL, Meyer T, Young MH. 2013. Airborne lidar on the Alaskan North Slope: wetlands mapping, lake volumes, and permafrost features. *The Leading Edge* **32**: 798–805.

Panda SK, Prakash A, Jorgenson MT, Solie DN. 2012. Near-surface permafrost distribution mapping using logistic regression and remote sensing in Interior Alaska.

GIScience and Remote Sensing **49**: 346–363.

Panda SK, Marchenko SS, Romanovsky VE. 2014. High-resolution permafrost modeling in Denali National Park and Preserve. National Park Service Report NPS/CAKN/NRTR–2014/858.

Pastick NJ, Jorgenson MT, Wylie BK, Minsley BJ, Ji L, Walvoord MA, Smith BD, Abraham JD, Rose JR. 2013. Extending airborne electromagnetic surveys for regional active layer and permafrost mapping with remote sensing and ancillary Data, Yukon Flats Ecoregion, Central Alaska. *Permafrost and Periglacial Processes* **24**: 184–199.

Pastick NJ, Jorgenson MT, Wylie BK, Nield SJ, Johnson KD, Finley AO. 2015. Distribution of near-surface permafrost in Alaska: estimates of present and future conditions. *Remote Sensing of Environment* **168**: 301–315.

Pearson RG, Phillips SJ, Loranty MM, Beck PSA, Damoulas T, Knight SJ, Goetz SJ. 2013. Shifts in Arctic vegetation and associated feedbacks under climate change. *Nature Climate Change* **3**: 673–677.

Post E, Bhatt US, Bitz CM, Brodie JF, Fulton TL, Hebblewhite M, Kerby J, Kutz SJ, Stirling I, Walker DA. 2013. Ecological consequences of sea-ice decline. *Science* **341**: 519–524.

Potapov P, Turubanova S, Hansen MC. 2011. Regional-scale boreal forest cover and change mapping using Landsat data composites for European Russia. *Remote Sensing of Environment* **115**: 548–561.

Potter C, Li S, Crabtree R. 2013. Changes in Alaskan tundra ecosystems estimated from MODIS greenness trends, 2000 to 2010. *Journal of Geophysics and Remote Sensing* **2**: 107.

Quinton WL, Hayashi M, Chasmer LE. 2011. Permafrost-thaw-induced land-cover change in the Canadian subarctic: implications for water resources. *Hydrological Processes* **25**: 152–158.

Raynolds MK, Walker DA, Verbyla D, Munger CA. 2013. Patterns of change within a tundra landscape: 22-year Landsat NDVI trends in an area of the northern foothills of the Brooks Range, Alaska. *Arctic Antarctic and Alpine Research* **45**: 249–260.

Raynolds MK, Walker DA, Ambrosius KJ, Brown J, Everett KR, Kanevskiy M, Kofinas GP, Romanovsky VE, Shur Y, Webber PJ. 2014. Cumulative geoecological effects of 62 years of infrastructure and climate change in ice-rich permafrost landscapes, Prudhoe Bay Oilfield, Alaska. *Global Change Biology* **20**: 1211–1224.

Regmi P, Grosse G, Jones M, Jones B, Anthony K. 2012. Characterizing post-drainage succession in thermokarst lake basins on the Seward Peninsula, Alaska with TerraSAR-X Backscatter and Landsat-based NDVI Data. *Remote Sensing* **4**: 3741–3765.

Reschke J, Bartsch A, Schlaffer S, Schepaschenko D. 2012. Capability of C-Band SAR for operational wetland monitoring at high latitudes. *Remote Sensing* **4**: 2923–2943.

Roach JK, Griffith B, Verbyla D. 2013. Landscape influences on climate-related lake shrinkage at high latitudes. *Global Change Biology* **19**: 2276–2284.

Rocha AV, Loranty MM, Higuera PE, Mack MC, Hu FS, Jones BM, Breen AL, Rastetter EB, Goetz SJ, Shaver GR. 2012. The footprint of Alaskan tundra fires during the past half-century: implications for surface properties and radiative forcing. *Environmental Research Letters* **7**: 044039.

Ropars P, Lévesque E, Boudreau S. 2015. How do climate and topography influence the greening of the forest-tundra ecotone in northern Québec? A dendrochronological analysis of Betula glandulosa. *Journal of Ecology* **103**: 679–690.

Rudy ACA, Lamoureux SF, Treitz P, Collingwood A. 2013. Identifying permafrost slope disturbance using multitemporal optical satellite images and change detection techniques. *Cold Regions Science and Technology* **88**: 37–49.

Sannel ABK, Kuhry P. 2011. Warming induced destabilization of peat plateau/thermokarst lake complexes. *Journal of Geophysical Research* **116**: G03035.

Saucier J-P, Baldwin K, Krestov PV, Jorgenson T. 2015. Boreal forests. In Routledge Handbook of Forest EcologyPeh *et al*. Taylor & Francis Group: New York; 7–29.

Schepaschenko D, McCallum I, Shvidenko A, Fritz S, Kraxner F, Obersteiner M. 2011. A new hybrid land cover dataset for Russia: a methodology for integrating statistics, remote sensing and in situ information. *Journal of Land Use Science* **6**: 245–259.

Schuur EAG, McGuire AD, Schädel C, Grosse G, Harden JW, Hayes DJ, Hugelius G, Koven CD, Kuhry P, Lawrence DM, Natali SM, Olefeldt C, Romanovsky VE, Schaefer K, Turetsky MR, Treat CC, Vonk JE. 2015. Climate change and the permafrost carbon feedback. *Nature* **520**: 171–179.

Segal RA, Lantz TC, Kokelj SV. 2016. Acceleration of thaw slump activity in glaciated landscapes of the Western Canadian Arctic. *Environmental Research Letters* **11**: 034025.

Selkowitz DJ, Stehman SV. 2011. Thematic accuracy of the National Land Cover Database (NLCD) 2001 land cover for Alaska. *Remote Sensing of Environment* **115**: 1401–1407.

Selkowitz DJ, Green G, Peterson B, Wylie B. 2012. A multi-sensor lidar, multi-spectral and multi-angular approach for mapping canopy height in boreal forest regions. *Remote Sensing of Environment* **121**: 458–471.

Serreze M, Barry RG. 2011. Processes and impacts of Arctic amplification: A research synthesis. *Global and Planetary Change* **77**: 85–96.

Short N, Brisco B, Couture N, Pollard W, Murnaghan K, Budkewitsch P. 2011. A comparison of TerraSAR-X, RADARSAT-2 and ALOS-PALSAR interferometry for monitoring permafrost environments, case study from Herschel Island, Canada. *Remote Sensing of Environment* **115**: 3491–3506.

Slater AG, Lawrence DM. 2013. Diagnosing present and future permafrost from climate models. *Journal of Climate* **26**: 5608–5623.

Soliman A, Duguay C, Saunders W, Hachem S. 2012. Pan-Arctic land surface temperature from MODIS and AATSR: Product development and intercomparison. *Remote Sensing* **4**: 3833–3856.

Steedman AE, Lantz TC, Kokelj SV. 2016. Spatio-temporal variation in high-centre polygons and ice-wedge melt ponds, Tuktoyaktuk Coastlands, Northwest Territories. *Permafrost and Periglacial Processes* DOI:10.1002/ppp.1880

Swanson DK. 2012. Monitoring of retrogressive thaw slumps in the Arctic Network, 2011: Three-dimensional modeling of landform change. National Park Service, Fort Collins, Colorado. Natural Resource Report NPS/ARCN/NRDS–2012/247.

Swanson DK. 2013a. Permafrost landforms as indicators of climate change in the Arctic Network of National Parks. *Alaska Park Science* **12**: 40–45.

Swanson DK. 2013b. Three decades of landscape change in Alaska's Arctic National Parks: Analysis of aerial photographs c. 1980-2010. National Park Service NPS/ARCN/NRDS–2014/669.

Tarasenko TV. 2013. Interannual variations in the areas of thermokarst lakes in Central Yakutia. *Water Resources* **40**: 111–119.

Terenzi J, Jorgenson MT, Ely CR. 2014. Storm-Surge flooding on the Yukon-Kuskokwim Delta, Alaska. *Arctic* **67**: 360–374.

Tremblay B, Levesque E, Boudreau S. 2012. Recent expansion of erect shrubs in the Low Arctic: evidence from Eastern Nunavik. *Environmental Research Letters* **7**: 035501.

Trofaier AM, Bartsch A, Rees WG, Leibman MO. 2013. Assessment of spring floods and surface water extent over the Yamalo-Nenets Autonomous District. *Environmental Research Letters* **8**: 045026.

Ulrich M, Grosse G, Strauss J, Schirrmeister L. 2014. Quantifying wedge-ice volumes in yedoma and thermokarst basin deposits. *Permafrost and Periglacial Processes* **25**: 151–161.

Urban M, Forkel M, Eberle J, Huettich C, Schmullius C, Herold M. 2014. Pan-Arctic climate and land cover trends from multivariate and multi-scale analyses (1981-2012). *Remote Sensing* **6**: 2296–2316.

Vermaire JC, Pisaric MFJ, Thienpont JR, Courtney-Mustaphi CJ, Kokelj SV, Smol JP. 2013. Arctic climate warming and sea ice declines lead to increased storm surge activity. *Geophysical Research Letters* **40**: 1–5.

Walker DA, Gould WA, Meier HA, Raynolds MK. 2002. The circumpolar arctic vegetation map. *International Journal of Remote Sensing* **23**: 2552–2570.

Walker DA, Leibman MO, Epstein HE, Forbes BC, Bhatt US, Raynolds MK, Comiso J, Gubarkov AA, Khomutov AV, Jia GJ, Kaarlejärvi E, Kaplan JO, Kumpula T, Kuss HP, Matyshak G, Moskalenko NG, Orechov P, Romanovsky VE, Ukraientseva NK, Yu Q. 2009. Spatial and temporal patterns of greenness on the Yamal Peninsula, Russia: interactions of ecological and social factors affecting the Arctic normalized difference vegetation index. *Environmental Research Letters* **4**: 045004.

Walter-Anthony KM, Zimov SA, Grosse G, Jones MC, Anthony PM, Chapin FS III, Finlay JC, Mack MC, Davydov S, Frenzel P, Frolking S. 2014. A shift of thermokarst lakes from carbon sources to sinks during the Holocene epoch. *Nature* **511**: 452–456.

Walvoord MA, Voss CI, Wellman TP. 2012. Influence of permafrost distribution on groundwater flow in the context of climate-driven permafrost thaw: Example from Yukon Flats Basin, Alaska, United States. *Journal of Water Resources* **48**: W07524.

Wang J, Sheng Y, Hinkel KM, Lyons EA. 2012. Drained thaw lake basin recovery on the western Arctic Coastal Plain of Alaska using high-resolution digital elevation models and remote sensing imagery. *Remote Sensing of Environment* **119**: 325–336.

Watts JD, Kimball JS, Jones LA, Schroeder R, McDonald KC. 2012. Satellite microwave remote sensing of contrasting surface water inundation changes within the Arctic–Boreal Region. *Remote Sensing of Environment* **127**: 223–236.

Westermann S, Duguay CR, Grosse G, Kääb A. 2015a. Remote sensing of permafrost and frozen ground. In Remote Sensing of the Cryosphere, Tedesco M (ed). John Wiley & Sons; 307–344.

Westermann S, Østby TI, Gisnås K, Schuler TV, Etzelmüller B. 2015b. A ground temperature map of the North Atlantic permafrost region based on remote sensing and reanalysis data. *The Cryosphere* **9**: 1303–1319.

Xu L, Myneni RB, Chapin FS III, Callaghan TV, Pinzon JE, Tucker CJ, Zhu Z, Bi J, Ciais P, Tømmervik H, Euskirchen ES, Forbes BC, Piao SL, Anderson BT, Ganguly S, Nemani RR, Goetz SJ, Beck PSA, Bunn AG, Cao C, Stroeve JC. 2013. Temperature and vegetation seasonality diminishment over northern lands. *Nature Climate Change* **3**: 581–586.

Zhang Y, Olthof I, Fraser R, Wolfe SA. 2014. A new approach to mapping permafrost and change incorporating uncertainties in ground conditions and climate projections. *The Cryosphere* **8**: 2177–2194.

Zeng H, Jia G. 2013. Impacts of snow cover on vegetation phenology in the Arctic from satellite view. *Advances in Atmospheric Sciences* **30**: 1421–1432.

